Fabrication of *Polygonatum cyrtonema* Hua Flavonoid-AgNPs and its PLA Composite Active Film for Extending the Shelf Life of Frozen Litchi

Zhihong Wang,[a] Song Wang,[a] Yingle Chen,[a] Liu Yang,[a] Zhiwen Qi,[b,*] and Lei Zeng [a,*]

This study presents an eco-friendly strategy to valorize *Polygonatum cryptonym* Hua flavonoids (PC) from the residues of polysaccharide extraction by synthesizing silver nanoparticles (PC-AgNPs) with enhanced bioactivity. Optimized synthesis (pH 7.5, 10 mM Ag^+, 55 °C, 30 min) yielded monodisperse, spherical PC-AgNPs (avg. 16.2 nm) with face-centered cubic crystal structure. Nanoparticles showed remarkable scavenging ability for DPPH free radical (SC_{50} = 2.61 μg/mL) and ABTS free radical (SC_{50} = 1.65 μg/mL) compared to the native PC samples. The PC-AgNPs were incorporated into polylactic acid (PLA) films (1% w/w), achieving superior mechanical performance (tensile strength: 54.6 MPa; elongation at break: 6.0%) while demonstrating broad-spectrum antimicrobial activity against *E. coli*, *S. aureus*, and *A. niger*. Mechanistic studies revealed that the nanocomposite film disrupted bacterial membrane integrity in *E. coli*. Applied to litchi preservation at -18°C, the 1%NPs/PLA coating effectively maintained mitochondrial enzyme activities (Succinate dehydrogenase, Cytochrome c oxidase, H^+-ATPase, Ca^{2+}-ATPase) at more than 80% of fresh fruit levels for a certain storage life, significantly delaying senescence compared to controls. These findings establish PC-AgNPs/PLA as a dual-functional active packaging material that synergistically combines antioxidant reinforcement, antimicrobial protection, and physiological regulation for postharvest fruit preservation.

DOI: 10.15376/biores.20.3.5279-5300

Keywords: Polygonatum cyrtonema Hua; Flavonoids; AgNPs; Antioxidant; Antimicrobial; Preservation

Contact information: a: Guangdong Provincial Key Laboratory of Silviculture, Protection and Utilization, Guangdong Academy of Forestry, Guangzhou, 510520, Guangdong, People's Republic of China; b: National Engineering Lab. for Biomass Chemical Utilization, Institute of Chemical Industry of Forest Products, Chinese Academy of Forestry, Nanjing 210042, Jiangsu, People's Republic of China;
** Corresponding authors: zhiwenqi89@163.com (Zhiwen Qi); gaflzeng@foxmail.com (Lei Zeng)*

INTRODUCTION

The core issues of postharvest decay of litchi include accelerated sugar decomposition (production of CO_2 or alcohols, aldehydes) caused by high respiratory intensity, and browning and decay caused by pathogen infection (such as litchi downy mildew). Its peel structure is special (lack of vascular bundles to directly connect the pulp), which leads to the inability to effectively replenish water after water loss and accelerates quality deterioration (Xu *et al.* 2025a). Although freezing preservation can extend the storage life of litchi, it may also allow for the presence of cold-resistant bacteria in the frozen environment. These bacteria can grow and reproduce normally under low temperature (-18 ^oC) (Yu *et al.* 2024). Furthermore, the appearance of rust-colored spots

in litchi flesh is a result of excessive oxidation, which alters both the color and flavor of litchi meat (Liang *et al.* 2015). Therefore, the research and development of new, environmentally friendly, and cost-effective biological preservatives will further advance the frozen litchi industry.

Silver nanoparticles (AgNPs) offer a broad antimicrobial spectrum and are considered environmentally safe, making them widely utilized in various applications (Qi *et al.* 2023). Traditionally, chemical reducing agents (such as dimethylformamide and sodium borohydride) have been employed to synthesize AgNPs; however, these agents can introduce biological toxicity (Pinu 2016). In contrast to biosynthesis methods, chemical and physical methods typically consume more energy and require a longer duration for nanoparticle preparation (Gong *et al.* 2024). The use of plant polyphenols for the synthesis of AgNPs presents significant advantages. Generally, natural flavonoids serve as reducing agents, capping agents, and stabilizers, facilitating the preparation of uniformly dispersed steady-state AgNPs. For instance, Yang *et al.* (2023) utilized polyphenols from camellia seed cake to synthesize AgNPs, which demonstrated a strong affinity for *Penicillium digitatum*, significantly reducing citrus decay. Similarly, Qi *et al.* (2023) employed fisetin derived from *Toxicodendron vernicifluum* to produce AgNPs with remarkable antioxidant and antimicrobial properties.

Among them, flavonoids possess multiple phenolic hydroxyl groups, a large π-bond conjugated system, and strongly coordinated oxygen atoms, which contribute to their significant chelating and bonding ability with Ag^+, resulting in the formation of flavonoid-AgNPs complexes (Qi *et al.* 2022c). Surprisingly, compared to the flavonoids themselves, the flavonoid-AgNPs complexes exhibit enhanced antioxidant and antimicrobial activities (Yang *et al.* 2023). Although biomass-derived flavonoids have been produced in large quantities, there is an urgent need to identify sources of food-borne flavonoids to control bacterial proliferation and preserve food freshness. It is worth noting that flavonoid secondary metabolites are environmentally friendly and avoid toxic residues of chemical reducing agents; their active components can be used as surface modifiers to endow NPs (Hussain *et al.* 2023) with antioxidant, antibacterial and other biological functions. Difference in the stereoisomers of flavanones can be used to regulate the crystal form of NPs (Hussain *et al.* 2023) (such as amorphous or face-centered cubic structure). *Polygonatum cyrtonema* Hua has been utilized as a daily ingredient and in traditional Chinese medicine to protect the kidneys, nourish yin, and alleviate fatigue (Nie *et al.* 2023). The plant is rich in flavonoids, including luteolin, kaempferol, and myricetin, which exhibit strong antioxidant, anti-inflammatory, and antimicrobial properties (Zhang *et al.* 2024). However, it has been reported that the solid waste produced after processing *Polygonatum cyrtonema* Hua still contains over 19 identified flavonoids, as determined by UPLC-Q Exactive-MS technology (Han *et al.* 2023). Currently, this waste is typically discarded, with only a small portion being utilized as food additives or animal feed. Therefore, the authors speculated that *Polygonatum cyrtonema* Hua flavonoids (PC) can reduce Ag^+ to Ag^0 through a quinone-phenol redox cycle to form a uniform particle size silver NPs.

Polylactic acid (PLA) is an ideal non-ionic polymer matrix that offers excellent biodegradability and biocompatibility (Liao *et al.* 2023). Through the synergistic effect of physical barrier, chemical antibacterial, and environmental regulation, antibacterial PLA film targeted to inhibit the key factors (respiratory metabolism, pathogens, and browning) of postharvest litchi (Mao *et al.* 2023; Shi *et al.* 2022). Wu *et al.* (2024) prepared three microstructures of AgNPs-PLA materials on electrospun PLA-thermoplastic polyurethane (TPU) nanofiber films by electro-spraying. The content of AgNPs was as low as 0.6 wt %,

and the highest antibacterial efficacy was 99 % ± 1 %. Mao *et al.* (2023) incorporated a 7 wt% anthocyanin-Cu complex into the PLA substrate, resulting in an antibacterial efficacy of 96.4% against *E. coli*. This active multilayer film effectively inhibits the rapid proliferation of bacteria in pasteurized milk, thereby extending its shelf life. Additionally, Xu *et al.* (2025b) introduced 6% anthocyanin into the PLA matrix, and the resulting electro-spun nanofiber film was employed to monitor the freshness of blueberries and prolong their shelf life. Pan *et al.* (2025) incorporated the extract of *Polygonati rhizoma* into the matrix of chitosan and soy protein isolate. The film effectively inhibited the growth of *Staphylococcus aureus* or *Escherichia coli* and showed complete biodegradability after 7 days.

The aim of this study was to extract PC from the solid waste residue of *Polygonatum cyrtonema* Hua and to prepare PC-AgNPs from the residue by using these PC as a template. The preparation conditions for the PC-AgNPs in the aqueous phase were screened. The structure of the PC-AgNPs was characterized, and their antioxidant and antimicrobial activities, along with the underlying mechanisms, were evaluated. Subsequently, co-filming with PLA was conducted to create an efficient, eco-friendly, and safe film (NPs/PLA) for the preservation of frozen litchi. This research is expected to provide practical guidance for the preparation of AgNPs and their incorporation into films with high antioxidant and antimicrobial properties, as well as for the further utilization of flavonoids derived from the residue of *Polygonatum cyrtonema* Hua.

EXPERIMENTAL

Materials

Polygonatum cyrtonema Hua was purchased from Meizhou Fudao Ecological Technology Co., Ltd. (Guizhou China). HPD-500 macroporous resin was obtained from Tianjin Yunkai Resin Technology Co., Ltd. (Tianjin, China). Other purchased chemicals included PLA (4032D, NatureWorks, Inc., USA), tri-n-butyl citrate (TBC, Aladdin Company, Shanghai, China), and dichloromethane (DCM, Shanghai Yuanye Bio-Technology Co., Ltd.). The polyamide resin and Sephadex LH-20 were purchased from Shanghai Yuanye Bio-Technology Co., Ltd. (Shanghai, China). DPPH (2,2-Di(4-tert-octylphenyl)-1-picrylhydrazyl), ABTS (2, 2'-azino-bis (3-ethylbenzothiazoline-6-sulfonic acid), and other biological kits were purchased from Nanjing Jiancheng Bioengineering Institute (Nanjing, China). The bacterial strains *Escherichia coli* (*E. coli*, ATCC 23815), *Staphylococcus aureus* (*S. aureus*, ATCC 12600), and *Bacillus subtilis* (*B. subtilis*, ATCC 6051), as well as the fungus *Aspergillus niger* (*A. niger*, ATCC 16404), were preserved by the Chinese Academy of Forestry. All other reagents were of analytical grade. The fruits of the tested 'Ziniangxi' litchi reached commercial maturity, with a transverse diameter of 3.5 cm and an average fruit weight of 22 g.

Isolation of flavonoids from PC

PC were extracted using an ultrasonic-assisted ammonium sulfate/ethanol aqueous two-phase method (Zhang *et al.* 2017). Briefly, the aqueous two-phase system comprised 24% ammonium sulfate and 30% anhydrous ethanol. The residue of *Polygonatum cyrtonema* Hua obtained after the extraction of polysaccharides was dried and weighed into the system according to a solid-liquid ratio of 1:20 (g/mL), and extracted for 30 min at an ultrasonic power of 340 W. After filtering and centrifuging the crude extract (6000 × *g* for

15 min) to remove the residue, the upper phase containing the flavonoid extract was collected by allowing it to stand in a liquid separation funnel.

The flavonoid extract obtained according to the above extraction process was concentrated using a rotary evaporator at 50 °C and purified with HPD-500 macroporous resin and polyamide resin. In summary, the flavonoids were enriched through a two-step column chromatography process. The enrichment experiments were conducted using an 80 mL chromatographic column (1 bed volume (BV), dimensions: 2.5 × 60 cm) filled with pre-treated HPD-500 macroporous resin in a wet loading configuration. The concentration of the sample solution was 2.0 mg/mL, and the sample flow rate was set at 1.5 BV/h. After the adsorption phase, elution fractions were collected using 50% and 70% ethanol (EtOH) solutions, which were then concentrated. The samples obtained through this process were subsequently treated with polyamide resin, and the target components were eluted using a 60% EtOH solution at a flow rate of 1.5 BV/h, and the concentrated extract was obtained by vacuum concentration.

In order to obtain a higher content of flavonoids in the concentrated extracts, the sample was further separated and purified using Sephadex LH-20 (Xue *et al.* 2019). After it was ensured that the above obtained sample had a suitable adsorption time with the chromatographic packing material, it was then eluted with a 60% methanol (MeOH) solution. The eluate was collected in 2.0 mL tubes. The flavonoid eluate was then concentrated under reduced pressure and freeze-dried to obtain enriched *Polygonatum cyrtonema* Hua flavonoids (Han *et al.* 2023). The content of the total flavonoids was determined using a spectrophotometry method and analyzed qualitatively using chromatography.

Aqueous Assembly Preparation of PC-AgNPs

Using a single-factor experiment, PC-AgNPs were prepared *via* the liquid-phase hydration method (Qi *et al.* 2022b). Briefly, the conditions for synthesizing PC-AgNPs by reducing $AgNO_3$ with a PC solution were screened. The PC solution at a concentration of 1.0 mg/mL was prepared, and $AgNO_3$ solutions of varying concentrations (1.0 to 10.0 mM) were added under different pH conditions ranging from 5.5 to 7.5. The pH of the solution was adjusted using H_3PO_4 and $NaBH_4$, and the mixture was thoroughly stirred with a magnetic stirrer. PC-AgNPs were synthesized over different reaction times of 1 to 60 min at temperatures between 25 and 65 °C. Upon completion of the reaction, a specific volume of the reaction mixture was removed, and the UV-visible absorption spectrum was scanned in the range of 200 to 800 nm to confirm the formation of PC-AgNPs. Based on the experiments, the preparation conditions of PC-AgNPs were obtained. Subsequently, acetone was added to the reaction solution, which was then centrifuged at 5000 × *g* for 20 min. The supernatant was discarded, and the precipitate was washed twice with deionized water. The resulting precipitate was dried at -40 °C with 0.05 mbar vacuum for 24 h to obtain PC-AgNPs samples.

Preparation of NPs/PLA Film

A series of NPs/PLA films were prepared using the solution casting method by simultaneously mixing PC-AgNPs and the plasticizer glycerol with PLA (Gao *et al.* 2019; Yadav *et al.* 2020). First, 1 g of PLA was dissolved in 20 mL of DCM and placed in a constant-temperature ultrasonic reactor. The PLA was completely dissolved using ultrasound for 0.5 h. The PC-AgNPs suspension was added dropwise to the PLA solution, and magnetic stirring was conducted for 1 h to ensure full dispersion and dissolution. Next,

TBC (20 wt%) was added to the solution, and the film-forming solution was obtained by continuing magnetic stirring for an additional time. Finally, the film-forming solution was poured and allowed to form at 55 °C with 0.05 mbar vacuum to prepare the NPs/PLA film.

Litchi Frozen Preservation Treatment

The packaging specifications were as follows: Single fruit weight: 20 ± 2 g, peel integrity ≥ 95%; composite film bag size: 15 × 20 cm (thickness 50 μm), heat sealing; contact area: the contact rate between the inner surface of the film and the peel is ≥ 80 % (achieved by pre-indentation treatment).

The thawing operation specifications were as follows: Thawing temperature: 4 °C refrigerated thawing for 12 h to avoid temperature spikes leading to cell rupture; storage conditions: After thawing, the samples were stored at 25 °C and 85% relative humidity for 6 h to simulate short-term shelf exposure. The NPs/PLA film sealed the litchi and was then stored at -18 °C. Samples were collected on the day of fruit storage and day 20, 40, 60, and 80. The litchi were frozen in liquid nitrogen, and stored at -18 °C.

Characterizations

High-Performance Liquid Chromatography (HPLC) was conducted using an Agilent 1260 Infinity II system (Agilent Technologies Co., Ltd., USA) equipped with an InfinityLab Poroshell 120 EC-C18 column (150 × 4.6 mm, 5 μm; Agilent, USA). Acetonitrile (Phase A) and a 2% formic acid-water solution (Phase B) as mobile phases was utilized as the analytical method. The elution gradient was established as follows: 5% A from 0 to 25 min, 22% A from 25 to 35 min, a gradient from 22% to 35% A from 35 to 50 min, a gradient from 35% to 5% A from 50 to 52 min, and 5% A from 52 to 55 min. The detection wavelength was set 320 nm, with an injection volume of 10 μL and a flow rate of 1.0 mL/min. Detection occurred at 40 °C. Flavonoids were extracted using an ultrasonic cleaning machine (SB-5200DT, Ningbo Scientz Biotechnology Co., Ltd.), and dried flavonoid samples were obtained using a vacuum freeze dryer (FD-A10N-50, Anhui NingHuai Instrument Co., Ltd.).

The ultraviolet-visible spectrophotometer (UV-Vis, Lambda 25, PerkinElmer, Germany) was utilized to record the ultraviolet-visible spectrum in the range of 200 to 800 nm, with a resolution of 1 nm. A multifunctional microplate reader (Spark 10 M, Tecan, Switzerland) was also employed. The particle size and potential were analyzed using the NanoZS90 particle size and potential analyzer (Malvern, UK). The Fourier Transform Infrared Spectrometer (FT-IR, FTS135, Bio-Rad, USA) was set to a wavelength range of 4000 to 400 cm^{-1}, with a resolution of 4 cm^{-1}. The particle size and morphology of the samples were examined using a scanning electron microscope (SEM, ZEISS Gemini 300, Zeiss, Germany) and a transmission electron microscope (TEM, H-7650, Hitachi, Japan) at 300 kV, with analysis performed using ImageJ software (Version 1.48, National Institutes of Health). The powder was analyzed using an X-ray powder diffractometer (XRD-6100, Shimadzu, Japan), with a CuKα radiation source, a current of 30 mA, a voltage of 40 kV, a scanning range of 10° to 80°, and a scanning speed of 2°/min.

DPPH and ABTS Free Radical Scavenging

According to the referenced literature method (Sun *et al.* 2020), with slight modifications, the ability of NPs to scavenge DPPH free radicals was assessed. Similarly, the capacity of NPs to scavenge ABTS free radicals was determined following the literature

method (Bretschneider *et al.* 2009), also with minor adjustments. The half maximal radical scavenging concentration (SC_{50}) of the sample was calculated using a standard curve.

Antimicrobial Activity of NPs/PLA Solution *in Vitro*

The minimum inhibitory concentration (MIC) was determined as described by Qi *et al.* (2023). Thawed *S. aureus*, *E. coli*, and *A. niger* were grown to the logarithmic phase and subsequently passaged. The bacterial concentration was diluted to 10^6 CFU/mL, and a negative control well was included. The MIC values for the bacteria were determined using the microbroth double dilution method on a 96-well microplate.

For morphological observation of bacteria, the broth culture of *E. coli* and *S. aureus* was prepared to achieve a 0.5 McBurney's turbidity standard using sterile water. NPs/PLA solution was then mixed with an equal volume of the bacterial solutions of *E. coli* and *S. aureus* at room temperature for 30 min. The samples were immobilized with glutaraldehyde and observed using scanning electron microscopy (SEM).

To determine the inhibition of bacterial respiratory chain dehydrogenase activity, *S. aureus* and *E. coli* were inoculated into broth culture medium. After 18 h of incubation, 0.5 mL of the broth culture was centrifuged at 4 °C and 16,000 × *g* for 30 min. The supernatant was discarded, and the bacterial pellet was washed once with normal saline. The bacterial precipitate was then mixed with the NPs/PLA solution at room temperature for 1 h. Concurrently, a living bacteria blank control (without PC-AgNPs) and a dead bacteria negative control (the dead bacteria were subjected to a water bath at 100 °C for 15 min to kill the bacteria and inactivate the respiratory chain dehydrogenase activity on the bacterial surface) were prepared. Following this, the samples were centrifuged at 16,000 × *g* and 4 °C for 30 min. The supernatant was discarded, and the pellet was washed once more with normal saline. Subsequently, 0.9 mL of PBS was added to the mixture, followed by the addition of the respiratory chain dehydrogenase substrate, 0.1 mL of 0.5% iodonitrotetrazolium methyl blue (INF). The reaction was allowed to proceed at 37 °C in the dark for 1 h. The absorbance at 490 nm of the reactants was measured using a microplate reader.

To detect bacterial cell membrane leakage, broth cultures of *S. aureus* and *E. coli* were prepared, and 0.5 mL of each culture was added to an Eppendorf tube. The samples were centrifuged at 16,000 × *g* and 4 °C for 30 min, after which the supernatant was discarded. The precipitate was then washed twice with sterile water. Following this, 1 mL of NPs/PLA solution was added to the precipitate. For the control group, 1 mL of sterile water was added instead. The mixtures were thoroughly mixed and incubated at 37 °C for 1 h. After incubation, the samples were centrifuged again at 16,000 × *g* and 4 °C for 30 min, and the supernatant was collected. The concentrations of protein and nucleic acids in the supernatant were measured using a nucleic acid and protein analyzer to assess the leakage of the bacterial cell membrane.

Determination of Enzyme Activities Related to Mitochondrial Energy Metabolism

The extraction of mitochondria from the mesocarp cell of litchi fruit was conducted using the method described by Silva *et al.* (2024), with some modifications. Briefly, 1.1 g of frozen litchi peel tissue was taken, and 10 mL of extraction buffer (50 mM Tris-HCl, pH 7.5, containing 1 mM EDTA, 0.25 M sucrose, 0.3 M mannitol, 0.5% PVP, 0.1% bovine serum albumin (BSA), and 0.1% cysteine, adjusted to pH 7.5 with 0.1 M concentrated hydrochloric acid) was added. The mixture was shaken thoroughly. The residue was then

filtered to obtain 6 to 7 mL of filtrate, which was centrifuged for 10 at 4,000 × *g* and 4 °C. The supernatant was centrifuged for 30 min at 16,000 × *g* and 4°C. After removing the supernatant, the precipitate was retained, and 1 mL of suspension buffer (10 mM Tris-HCl, pH 7.5, containing 0.25 M sucrose, 0.3 M mannitol, and 1 mM EDTA) was added to dissolve the precipitate. The crude mitochondrial extract was then obtained and stored at 4 °C for subsequent testing.

Mitochondrial H^+-ATPase activity was determined as previously described (Zhao *et al.* 2023). Mitochondrial Ca^{2+}-ATPase activity was measured as described by Lyu *et al.* (Lyu *et al.* 2019), with slight adjustments. The activity of mitochondrial succinate dehydrogenase (SDH) was measured using the method described by Montagut *et al.* (Montagut *et al.* 2022), with slight modifications. Mitochondrial cytochrome C oxidase (CCO) activity was measured as described by Montagut *et al.* (2022), with slight adjustments.

In vivo Cytotoxicity

Referring to the report by Yang *et al.* (2020), LO2 cells in logarithmic growth phase were taken, and the cell density was adjusted to 5×10^4 cells/mL by RPMI-1640 medium (containing 10% fetal bovine serum), and inoculated into 96-well plates (100 μL/well). Appropriate amounts of samples were added and incubated at 5% CO_2 and 37°C for 24 h. 5 mg/mL MTT solution (100 μL) was added to each well. After 4 h of incubation, the supernatant was discarded, and DMSO (150 μL/well) was added to dissolve the formazan crystals. The absorbance at 490 nm wavelength was measured by microplate reader, and the cell survival rate was calculated.

Data Analysis

All experimental data are presented as mean ± standard deviation (x ± s) based on three-fold replication. Origin 9.0 and GraphPad Prism 8 software were utilized for graphical representation, while SPSS software was employed for significance analysis. For functional evaluation of PC-AgNPs, a p-value of less than 0.05 ($p < 0.05$) was established as the threshold for statistical significance.

RESULTS AND DISCUSSION

Optimization Preparation of PC-AgNPs

The yield of the PC prepared using the ultrasound-assisted ammonium sulfate/ ethanol aqueous two-phase method was (1.12 ± 0.29)%. After further enrichment and purification with HPD-500 macro-porous resin, polyamide resin, and Sephadex LH-20, the content of the PC increased to (92.6 ± 0.18)%, free from polysaccharides, proteins, and other impurities (Fig. 1A). The freeze-dried sample of the PC appeared as a yellow solid. Plant polyphenols are secondary metabolites characterized by a polyphenolic structure, which exhibit strong reducing capabilities and possess certain antimicrobial activities. They can effectively convert silver salts into elemental silver (Qi *et al.* 2023). When the PC were dissolved in deionized water and mixed with $AgNO_3$ and $NaHB_4$, the color of the mixture changed from colorless to white. This color change indicates that the silver ions were being reduced to form PC-AgNPs particles (Li *et al.* 2023), resulting in the freeze-dried sample appearing as a black solid. The effects of various reaction factors (pH, Ag^+ concentration, reaction temperature and reaction time) on the formation of nanoparticles were as follows:

Solution pH

As illustrated in Fig. 1B, the maximum absorption value increases with rising pH levels, indicating that alkaline conditions favor the synthesis of PC-AgNPs. The primary reason for this is that under alkaline conditions (pH 7.5), the reducing hydroxyl groups of PC are more likely to lose protons, resulting in a negatively charged molecule. This negatively charged polyphenolic compound not only interacts more readily with Ag^+ ions, but also facilitates the transfer of electrons to Ag^+, leading to the formation of PC-AgNPs. These findings are consistent with the results reported by Fan *et al.* (2021).

Ag^+ concentration

Nano-silver exhibits a characteristic absorbance peak in the wavelength range of 400 to 450 nm. As shown in Fig. 1C, there was a distinct absorbance peak near 450 nm, confirming the presence of nano-silver. At a concentration of 1 mM Ag^+, no significant absorbance peak was observed. However, when the concentration increased to 2 mM, the absorbance peak diminished, and the half-peak width broadened. This may be attributed to the presence of additional reducing agents in the reaction which interferes with the detection of nano-silver, similar to the findings reported by Mohaghegh *et al.* (2020). As the concentration rose from 5 to 10 mM, the intensity of the absorption peak increased, indicating a corresponding rise in the concentration of PC-AgNPs. Nevertheless, the absorbance peak exhibited a red shift, and the half-peak width increased, suggesting that the particle size of the generated PC-AgNPs gradually increased and that the size distribution became more heterogeneous. When the concentration of Ag^+ continued to rise, the reduction rate of silver ions no longer increased due to the limitations of the reducing capacity of PC. Consequently, 10 mM was identified as the optimal Ag^+ concentration for the preparation of PC-AgNPs.

Reaction temperature

As shown in Fig. 1D, the results indicated that as the reaction temperature increased from 25 to 65 °C, the intensity of the absorption also increased. This suggests that the concentration of PC-AgNPs rose with the increasing mixing temperature. However, when the temperature continued to rise beyond 65 °C, the absorbance peak exhibited a red shift, and the half-peak width broadened. This change indicates that the particle size of the generated PC-AgNPs gradually increased, resulting in an uneven distribution, as reported by Dong *et al.* (2020). Consequently, 55 °C was selected as the optimal reaction temperature for the preparation of PC-AgNPs.

Reaction time

As illustrated in Fig. 1E, the effects of varying mixing times on the UV-Vis absorption spectrum were evaluated under optimized conditions. As the reaction time increased from 1 min to 60 min, the maximum absorption value initially rose and then declined; however, the overall change was not significant, consistent with Na-Phatthalung's findings (Na-Phatthalung *et al.* 2022). This indicates that the maximum absorbance value slightly decreased with prolonged reaction time. A possible explanation for this phenomenon is that extended mixing times may disrupt the structure of the PC, resulting in a reduction of PC-AgNPs content. Consequently, 30 min was determined to be the optimal reaction time for the preparation of PC-AgNPs.

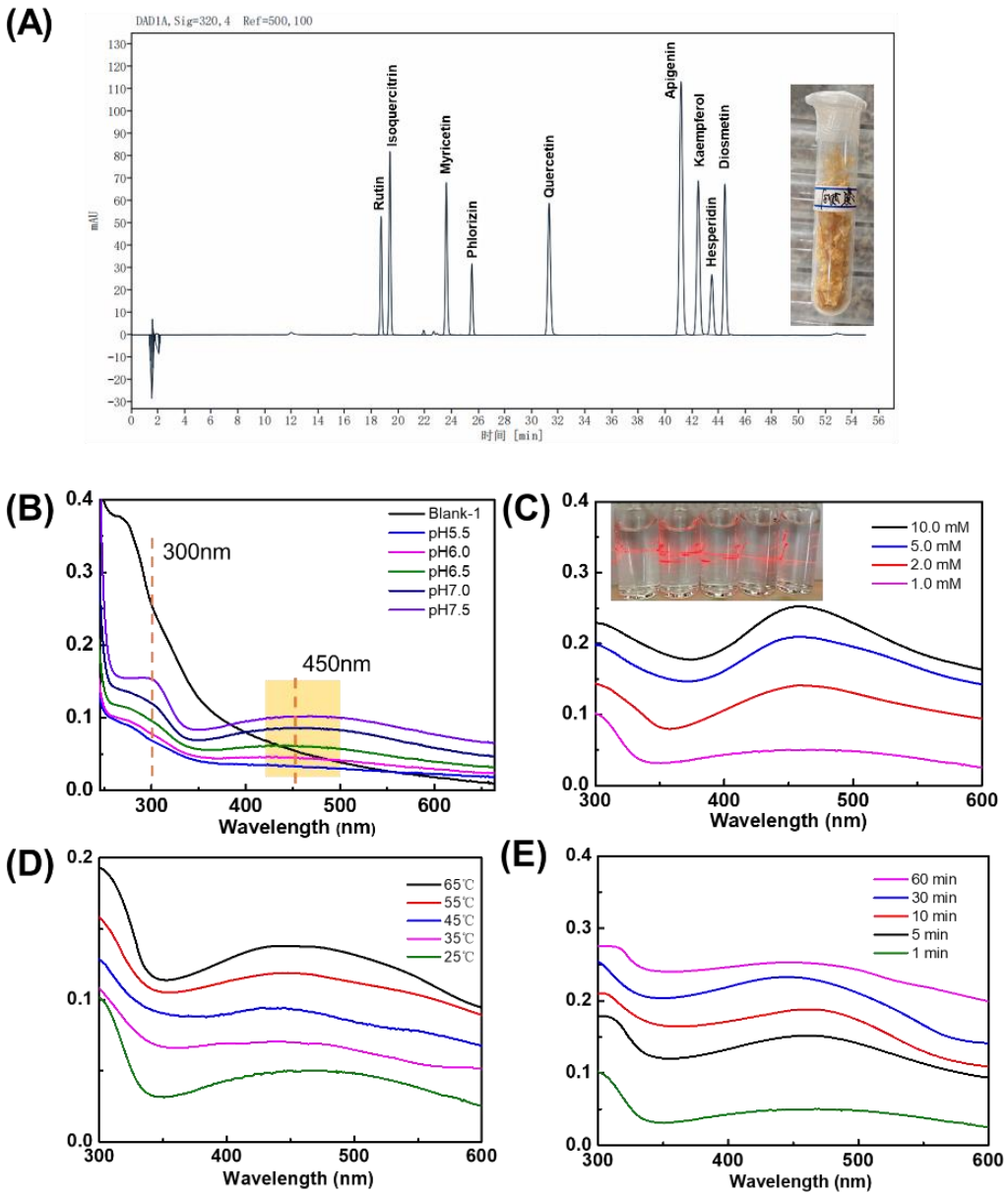

Fig. 1. HPLC spectrum of PC (A), and the formation of PC-AgNPs; along with their UV-Vis spectra, were recorded under varying conditions: reaction pH (B), $AgNO_3$ concentration (C), temperature (D), and time (E). * The mobile phase consisted of acetonitrile and a 2% formic acid solution, with the detection wavelength set at 320 nm.

Morphologies

As shown in Fig. 2A, the dried PC-AgNPs were observed to be nearly circular under SEM. The results also indicated that the PC-AgNPs synthesized from PC exhibited good dispersibility. As revealed in Fig. 2B, the aggregation of PC-AgNPs particles was significantly reduced, with the AgNPs independently distributed in the field of view. Therefore, the results indicate that the PC-AgNPs prepared in this study maintained an approximate spherical shape, uniform size, and good dispersion. Subsequently, 200 dots of PC-AgNPs within the image range were selected for analysis to determine the particle size. The diameter distribution of the synthesized PC-AgNPs ranged from 5 to 45 nm, with an average diameter of 16.2 nm and a standard deviation of 2.88 nm. The histogram indicated

that the majority of PC-AgNPs had diameters between 10 and 25 nm, corresponding to a narrow and uniform distribution. The average size of the AgNPs was 14.9 nm, with a standard deviation of 1.08 nm (Fig. 2B). The interaction between the functional groups in the PC and the AgNPs resulted in strong electrostatic repulsion among the PC-AgNPs, preventing the aggregation of the nanoparticles and facilitating the formation of a stable and dispersed spherical structure. Furthermore, as illustrated in Fig. 2(C-D), the atomic percentages in the sample were 30.4% Ag, 58.8% C, and 10.9% O, respectively, with no interference signals from other elements, indicating a high level of purity in the system. The element Ag exhibited distinct signal absorption peaks at 3.0 and 3.18 keV (within the range of 2.5 to 3.5 keV), and the main absorption peak was located at 3.0 keV. This confirms that Ag^{+} has been reduced to its elemental form, which is consistent with the findings reported in the literature by Qi *et al*. (2022c, 2023).

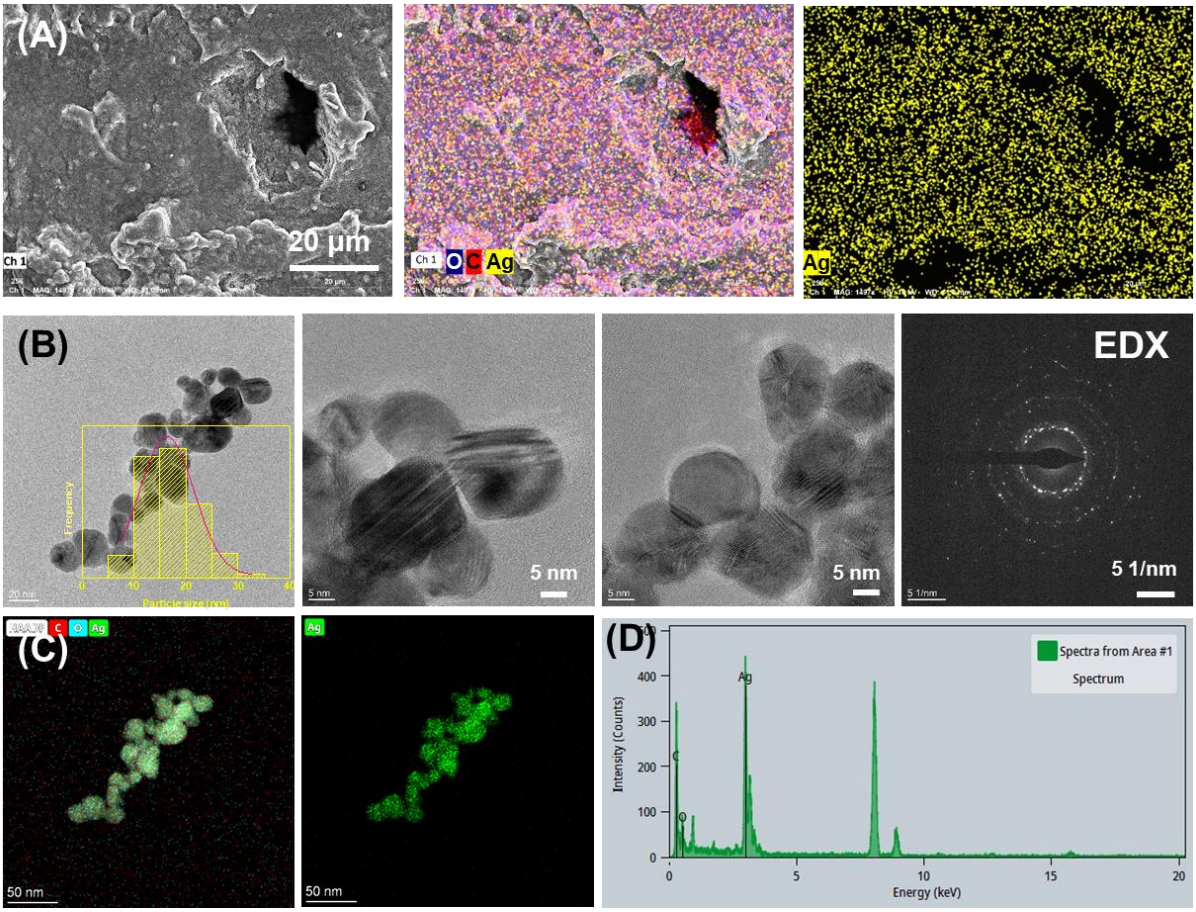

Fig. 2. SEM micrographs (A), TEM micrographs and EDX (B), elemental mapping (EDS), and the element point diagram for C, O, and Ag (C), along with the EDS spectrum (D) of PC-AgNPs. * Except for the variables in each group, the other fixed parameters were pH 7.5, $AgNO_3$ concentration of 10.0 mM, a reaction temperature of 55 °C and a reaction time of 30 min. The morphologies and yields of PC-AgNPs served as standards and indicators of the preparation process.

FT-IR

As illustrated in Fig. 3A, the Fourier Transform Infrared (FT-IR) spectra of PC-AgNPs and PC exhibit notable similarities. In contrast, AgNPs displayed minimal absorbance peaks in the functional group region. Both PC and PC-AgNPs demonstrated

characteristic absorbance features; however, the PC sample presented a deformation vibration peak associated with the phenolic hydroxyl group at 1398 cm^{-1}. Compared to PC, the deformation vibration peak of the phenolic hydroxyl group in PC-AgNPs was weakened.

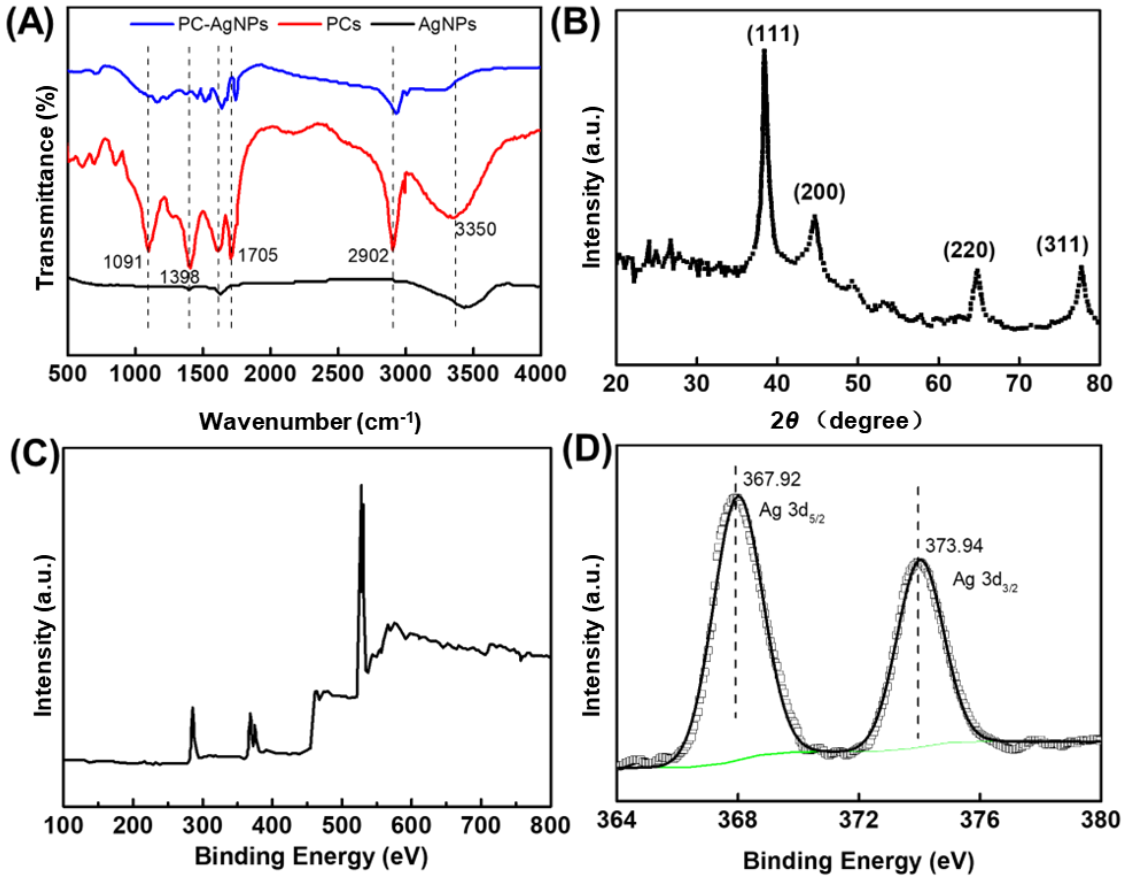

Fig. 3. FT-IR spectrum (A), XRD spectrum (B), XPS spectrum (C), and the enlarged XPS spectrum of AgNPs (D)

In the FT-IR spectra of PC, the absorbance peaks at 3350, 2902, and 1705 cm^{-1} correspond to the stretching vibrations of the O-H, C-H, and C=O groups, respectively. When interacting with Ag^{+}, the absorbance peak shifted to 3303 cm^{-1}, and its intensity significantly decreased while becoming broader. This suggests a hydrogen bond-like interaction between the O-H group of PC and the silver atoms in silver nanoparticles (O-H···Ag), indicating that PC may participate in the reduction process. The stretching vibration peak of O-H changed from 3350 cm^{-1} (PC) to 3297 cm^{-1} (PC-AgNPs). This finding aligns with previous literature (Sathiyaseelan *et al.* 2020), suggesting an interaction between the O-H group on the PC molecule and AgNPs, leading to the formation of a new O-Ag bond. The absorption bands at 1613, 1398, and 1091 cm^{-1} correspond to the stretching vibration of conjugated carbonyl (C=O), the bending vibration of C-H, and the skeletal vibration of the aromatic ring. These absorbance peaks primarily originated from PC. Similar characteristic absorbance peaks were also observed in the FT-IR spectrum of camellia seed cake polyphenols-AgNPs (Yang *et al.* 2023), where many absorbance peaks were blue-shifted compared to those of PC, and the peak intensity was reduced, indicating the formation of PC-AgNPs.

XRD and XPS

As shown in Fig. 3B, there were no sharp or narrow diffraction peaks, indicating that the PC-AgNPs had an amorphous structure (Ullah *et al.* 2021). The diagram reveals three diffraction peaks at 38.7°, 64.4°, and 77.8°, which correspond to the (111), (220), and (311) planes of the face-centered cubic phase of the silver crystal structure, respectively. This suggests that PC can reduce Ag^{+} to produce Ag^{0} (Qi *et al.* 2023). The significant broadening of the diffraction peaks is attributed to the very small microcrystalline size, and the peaks appear relatively cluttered in the diagram (Iezzi *et al.* 2022). This may be due to the dispersion of PC, resulting in a substantial number of PC being wrapped around the surface of the generated PC-AgNPs.

In addition, Fig. 3(C, D) shows two peaks at 367.92 eV and 373.9 eV, corresponding to Ag $3d_{5/2}$ and $Ag3d_{3/2}$, respectively. This finding further suggests that PC can act as reducing agents in the synthesis of PC-AgNPs nanoparticles, with the proportion of Ag 3d atoms in the synthesized polyphenol AgNPs being 2.92%. The study by Asmat-Campos *et al.* (2020) also demonstrated that the peaks in the XRD and XPS patterns were complex due to the interference of biological organic reagents or bioactive compounds on the surface of PC-AgNPs.

DPPH and ABTS Free Radical Antioxidant Activity Evaluation

As shown in Table 1, the SC_{50} values of PC and PC-AgNPs against DPPH and ABTS radicals were 3.87 and 2.61 μg/mL, and 2.35 and 1.65 μg/mL, respectively. The results indicate that the ability of free PC to scavenge DPPH and ABTS free radicals was significantly weaker than that of the PC-loaded AgNPs system. The nano-crystallization process enhanced the solubility of PC, facilitated their interaction with free radicals in aqueous solution, and improved the antioxidant activity of PC (Bretschneider *et al.* 2009).

Table 1. Inhibition Zone Against Tested Bacterial and Fungal Strains and Antioxidant Property of PC-AgNPs

	MIC value (μg/mL)				SC_{50} (μg/mL)	
Samples	*E. coli*	*S. aureus*	*B. subtilis*	*A. niger*	DPPH	ABTS
PC	56.29±1.89**	66.27±1.87**	55.28±1.57**	64.75±1.87**	3.87	2.35
PC-AgNPs	6.28±0.38	8.28±0.57	7.28±0.42	9.28±0.38	2.61	1.65
Cefixime	4.28±0.28	9.58±0.67	6.87±0.46	NT	NT	NT
Fluconazole	NT	NT	NT	5.26±0.26	NT	NT
* "NT" stands for Not Tested						

Mechanical Properties of NPs/PLA Film

Compared to smooth and flat pure PLA film, when the content of nanoparticles (NPs) in the PLA exceeded 1.0%, distinct markings began to appear on the surface of the NPs/PLA composite film, as shown in Fig. 4(A-B). Furthermore, a higher concentration of NPs in the PLA resulted in a more pronounced honeycomb structure. This phenomenon can be attributed to the increased crosslinking density caused by the higher amounts of NPs. The thickness of the pure PLA film was approximately 40 μm, as indicated in Fig. 4(C-D). After the addition of NPs and TBC, the film thickness increased to about 73 μm. Notably, there was no fracture layer observed in the fracture cross-section of the NPs/PLA composite film, which may be due to the interaction between the NPs and the PLA matrix, thereby enhancing the compatibility between the two materials. When 1.0% NPs were

added, the maximum tensile strength increased to 54.6 MPa, surpassing that of pure PLA film (Fig. 4E). The elongation at break of the composite film decreased from 6.2% to 4.5% as the mass percentage of NPs increased. This indicates that the elongation at break was influenced by the compatibility between the NPs and PLA. Furthermore, the Young's modulus of the composite film rose from 1.78 to 2.32 GPa (Fig. 4F).

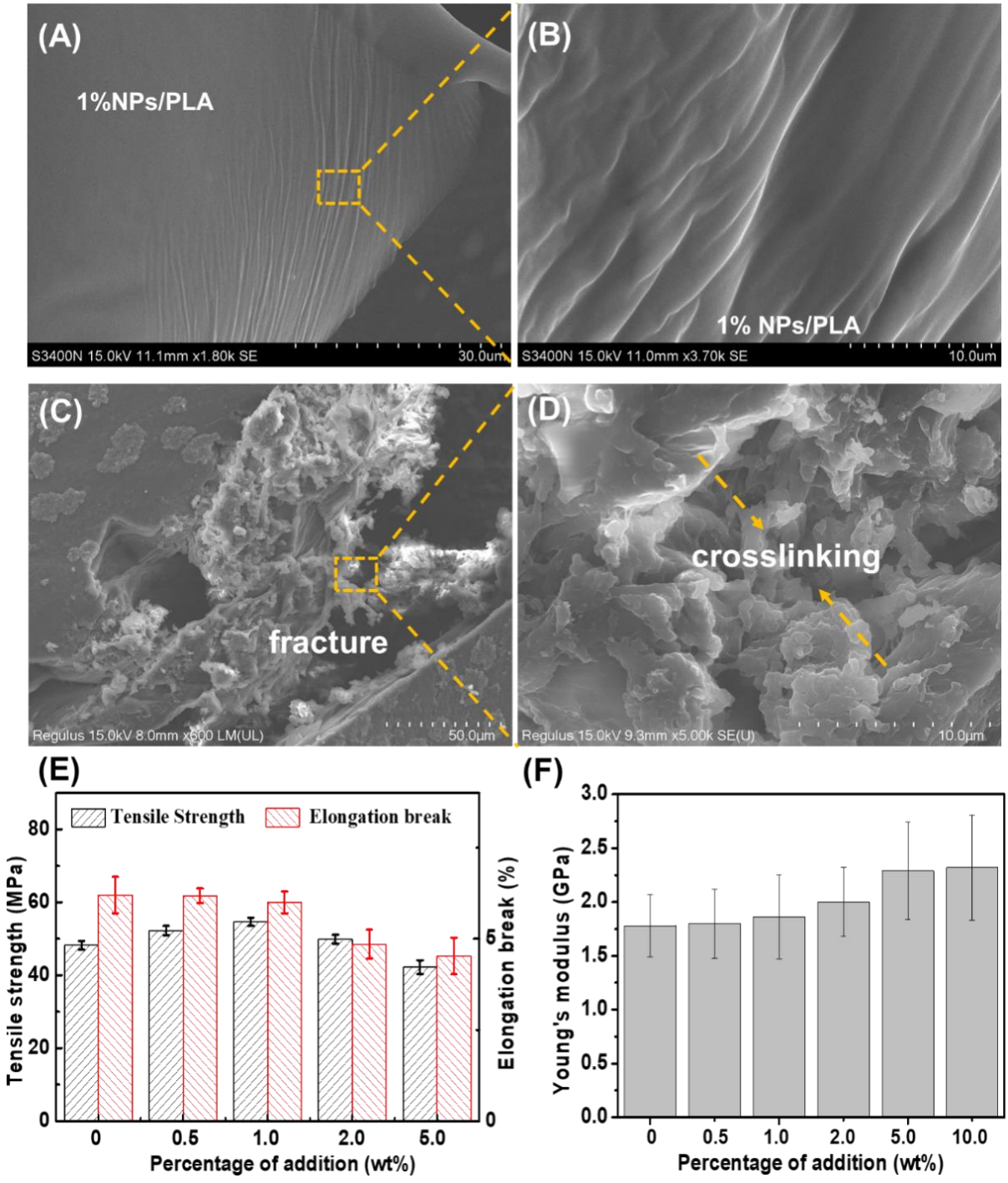

Fig. 4. The surface morphology (A-B), cross-sectional morphology (C-D), stress and tensile strength (E), and Young's modulus (F) of NPs/PLA

Antimicrobial Activity

As shown in Table 1, the results indicate that PC-AgNPs exhibited significant antimicrobial activity against *S. aureus*, *E. coli*, *B. subtilis*, and *A. niger*. Notably, PC-AgNPs demonstrated the strongest antimicrobial effect against *E. coli*. At a concentration of 6.28 mg/mL, PC-AgNPs were able to inhibit the growth of this bacterium. This efficacy can be attributed to the small size and large surface area of the PC-AgNPs, which facilitate the disruption of bacterial cell wall structures and enable the particles to penetrate the cells, thereby inhibiting bacterial growth. The proportion of atoms on the surface of silver nanoparticles (AgNPs) increases significantly at the nanoscale, and the uncoordinated atoms on the surface can be used as free radical capture sites to decompose reactive oxygen species (ROS) by electron transfer or catalysis (Qi *et al.* 2022a). The surface plasmon resonance characteristics of AgNPs in the ultraviolet-visible region may promote photocatalytic reactions and enhance the ability to scavenge specific ROS (such as superoxide anions) (da Silva *et al.* 2020). This finding is consistent with Wu *et al.* (2021).

As illustrated in Fig. 5(A-B), after treatment with the NPs/PLA solution for 1 h, the morphology of *E. coli* and *S. aureus* was examined using Bio-SEM (Adame *et al.* 2024). A significant number of PC-AgNPs were adsorbed onto the surfaces of both *E. coli* and *S. aureus*. The surface structures of normal *E. coli* and *S. aureus* were distinct, with the microcapsules clearly visible. However, the presence of PC-AgNPs disrupted the surface structures of both bacteria, resulting in partially defective microcapsules. Furthermore, while the surface structures of normal *E. coli* and *S. aureus* were well-defined, the introduction of PC-AgNPs altered these structures. The bacteria exhibited damage characterized by a hollow appearance, leading to the formation of bacteria, with indistinct cell edges, which aligns with Bhan and Golder (2023).

As illustrated in Fig. 5C, the results indicated that the respiratory chain dehydrogenase activity of *E. coli* and *S. aureus* in the live bacteria control group was significantly high, with the catalytic substrate INF producing distinct red compounds. In contrast, the respiratory chain dehydrogenase activity of *E. coli* and *S. aureus* in both the NPs/PLA solution experimental group and the dead bacteria control group (heat sterilization group) was markedly reduced ($p < 0.05$). The inhibition efficacy of PC-AgNPs on the respiratory chain dehydrogenase activity of *E. coli* and *S. aureus* approached 100%. These findings demonstrate that the NPs/PLA solution effectively inhibited the respiratory chain dehydrogenase activity of *E. coli* and *S. aureus*, which aligns with Gomaa (2017).

The mechanism of antibacterial activity was determined by examining the destruction of bacterial cell film and the leakage of cytoplasmic contents caused by AgNPs (Saratale *et al.* 2020). Broth cultures of *E. coli* and *S. aureus* were centrifuged and washed at high speed. The bacterial precipitates were collected and treated with 1 mL of NPs/PLA solution at specified final concentrations. The control group received 1 mL of sterile water and was mixed thoroughly. After incubation at 37°C for 1 h, the supernatant was centrifuged at high speed. The protein and nucleic acid content in the supernatant was analyzed using a nucleic acid protein analyzer. The experimental results indicated that when the concentration of sample was 1%NPs/PLA, the cell membranes of *S. aureus* were affected, and the cell membranes were compromised when the concentration of 5% NPs/PLA was reached, which caused significant leakage of proteins (Fig. 5D), DNA (Fig. 5E), and RNA (Fig. 5F) from the bacterial cells.

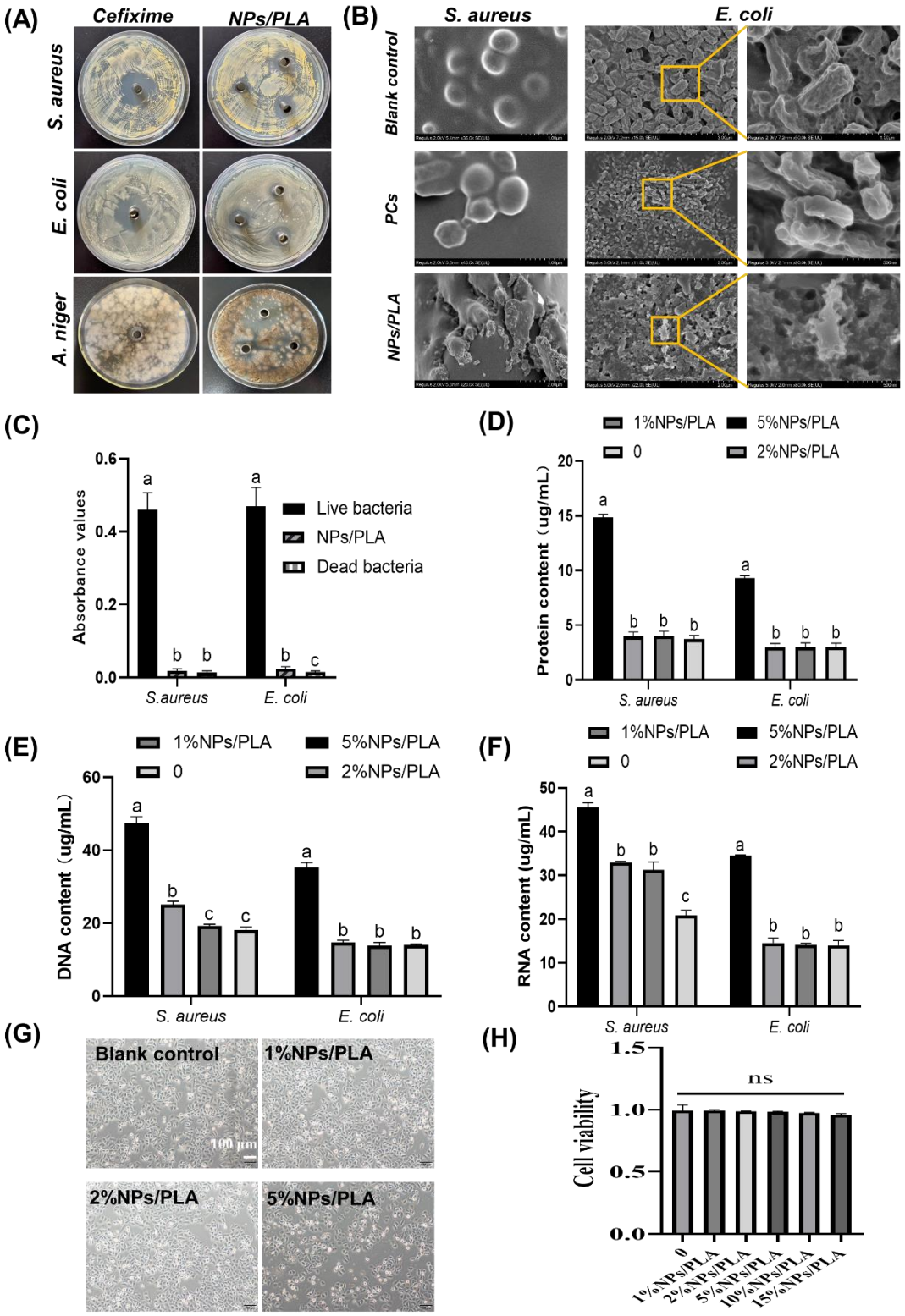

Fig. 5. The inhibition ratio of various concentrations (μg/mL) of NPs/PLA solution on bacteria and fungi (A), along with enlarged images of the damaged morphologies (B), the inhibitory effect of the novel NPs/PLA solution on bacterial respiratory chain dehydrogenase activity (C), UV absorbance, protein content (D), DNA content (E), and RNA content (F), as well as the morphology (G) and relationship (H) of different concentrations of NPs/PLA solution on LO2 cells.

In-vitro Toxicity

In the described exposure system, the external or internal dissolution of NPs/PLA will continuously release Ag^+ ions, making it essential to assess their cytotoxicity (Khin *et al.* 2024). As illustrated in Fig. 5(G-H), the cell viability of LO2 cells co-incubated with various concentrations of the NPs/PLA solution was evaluated using the MTT assay. The results indicated that the cell survival rate exceeded 95% within the tested maximum concentration range (15%NPs/PLA), suggesting that the NPs/PLA exhibit excellent cell compatibility.

Activities of Enzymes Related to Mitochondrial Energy Metabolism

As illustrated in Fig. 6, the activities of H^+-ATPase, Ca^{2+}-ATPase, SDH, and CCO in the control group exhibited a downward trend during storage. The rate of decline in mitochondrial energy metabolism-related enzyme activity in the four cells of litchi fruit treated with 1%NPs/PLA was significantly lower than that in the control group. Specifically, the activity of H^+-ATPase in the mitochondria of litchi fruit gradually decreased (Fig. 6A). This decline may be attributed to the limitations in the respiratory metabolism of the mitochondria, which results in reduced ATP synthesis and, consequently, diminished H^+-ATPase activity. The activity of Ca^{2+}-ATPase also decreased (Fig. 6B) with storage periods longer than 40 days.

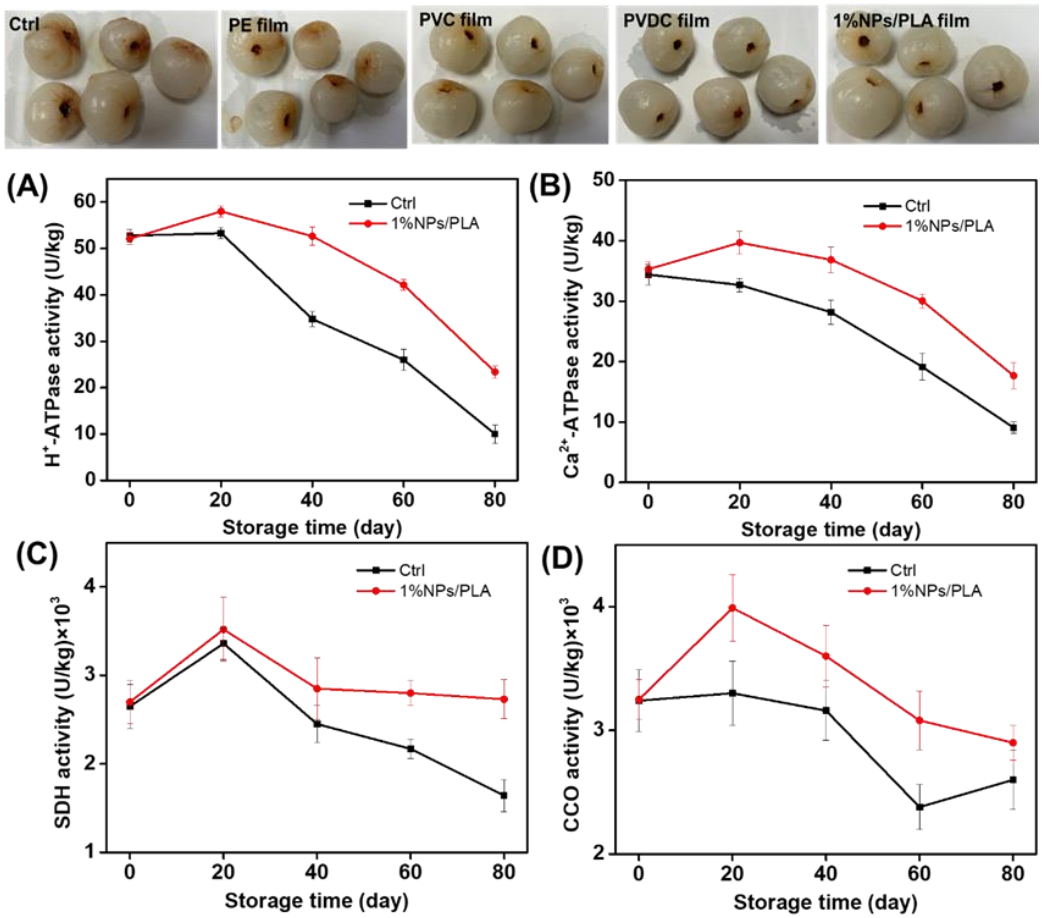

Fig. 6. Effect of different treatments on H^+-ATPase (A), Ca^{2+}-ATPase (B), SDH(C), and CCO (D) activities in 'Ziniangxi' litchi fruit. Note: polyethylene (PE), polyvinylchlorid (PVC), polyvinylidene chloride (PVDC).

The activity of Ca^{2+}-ATPase in the mitochondria decreased relatively less during the later stages of cryopreservation, which may lead to an increase in Ca^{2+} content within the mitochondria. Additionally, the activity of the SDH enzyme decreased (Fig. 6C). Notably, SDH maintained a high enzyme activity after 40 days of low temperature storage (-18 ℃) of litchi fruits, indicating that the mitochondria in the fruits at this stage were in a good functional state. After 40 days of cryopreservation, the CCO enzyme activity in litchi fruit remained elevated, suggesting that the oxygen consumption rate in the fruit was also high, reflecting an increased level of respiratory metabolism in the mitochondria at this time. However, after 60 days, the activity of the CCO enzyme decreased significantly (Fig. 6D), indicating a decline in aerobic respiration metabolism within the mitochondria of the fruit. This decline may lead to electron leakage in the mitochondrial respiratory chain, resulting in an increase in reactive oxygen species in the fruit.

CONCLUSIONS

1. Bio-sourced silver nanoparticles were successfully synthesized through flavonoid-mediated reduction using high-purity phytochemicals from *Polygonatum cyrtonema* Hua. The particles (PC-AgNPs) demonstrated remarkable efficacy in delaying postharvest senescence of litchi fruit by modulating physiological metabolic pathways. PC-AgNPs exhibited superior colloidal stability and narrower size distribution. Notably, PC-AgNPs showed enhanced antioxidant capacity and broad-spectrum antimicrobial activity, with significantly larger inhibition zones against *Escherichia coli*, *Staphylococcus aureus*, and *Aspergillus niger*.
2. Mechanistic investigations elucidated that PC-AgNPs exerted antimicrobial effects through dual action: structural disruption of microbial cell walls/membranes and induction of membrane hyperpermeability. This dual mechanism triggered substantial leakage of intracellular ATP and proteins, coupled with inhibition of dehydrogenase activity, ultimately leading to microbial cell death. Interfacial hydrogen bonding between PC-AgNPs and polylactic acid significantly improved material compatibility, enhancing film flexibility with increased elongation at break.
3. These findings establish PC-AgNPs as a multifunctional nanomaterial with dual applications in food preservation and active packaging, providing both mechanistic insights and practical solutions for postharvest quality management.

ACKNOWLEDGMENTS

This work was supported by the Guangdong Forestry Science and Technology Innovation Project (Grant No. 2021KJCX004), and the National Key Research and Development Program of China (Grant No. 2022YFD2200604-3).

REFERENCES CITED

Adame, M. Y., Wang, Y., Shi, C., Aziz, T., Al-Asmari, F., Sameeh, M. Y., Cui, H., and Lin, L. (2024). "Fortification of pullulan/cassava starch-based edible films incorporated with LC-EO nanoparticles and the application for beef meat preservation," *International Journal of Biological Macromolecules* 279, article 135629. DOI: 10.1016/j.ijbiomac.2024.135629

Asmat-Campos, D., Abreu, A.C., Romero-Cano, M.S., Urquiaga-Zavaleta, J., Contreras-Cáceres, R., Delfín-Narciso, D., Juárez-Cortijo, L., Nazario-Naveda, R., Rengifo-Penadillos, R., and Fernández, I. (2020). "Unraveling the active biomolecules responsible for the sustainable synthesis of nanoscale silver particles through nuclear magnetic resonance metabolomics," *ACS Sustainable Chemistry & Engineering* 8(48), 17816-17827. DOI: 10.1021/acssuschemeng.0c06903

Bhan, C., and Golder, A. K. (2023). "Utilizing bioinspired AgNPs as an antibacterial agent to enhance ceramic membrane performance," *Journal of Environmental Chemical Engineering* 11(3), article 110283. DOI: 10.1016/j.jece.2023.110283

Bretschneider, J. C., Reismann, M., von Plessen, G., and Simon, U. (2009). "Photothermal control of the activity of HRP-functionalized gold nanoparticles," *Small* 5(22), 2549-2553.

da Silva, R. T. P., Petri, M. V., Valencia, E. Y., Camargo, P. H. C., de Torresi, S. I. C., and Spira, B. (2020). "Visible light plasmon excitation of silver nanoparticles against antibiotic-resistant *Pseudomonas aeruginosa*," *Photodiagnosis and Photodynamic Therapy* 31, article 101908. DOI: 10.1016/j.pdpdt.2020.101908

Dong, B., Liu, G., Zhou, J., Wang, J., and Jin, R. (2020). "Transformation of silver ions to silver nanoparticles mediated by humic acid under dark conditions at ambient temperature," *Journal of Hazardous Materials* 383, article 121190. DOI: 10.1016/j.jhazmat.2019.121190

Fan, M., Si, J., Xu, X., Chen, L., Chen, J., Yang, C., Zhu, J., Wu, L., Tian, J., Chen, X., Mou, X., and Cai, X. (2021). "A versatile chitosan nanogel capable of generating AgNPs in-situ and long-acting slow-release of Ag^+ for highly efficient antibacterial," *Carbohydrate Polymers* 257, article 117636. DOI: 10.1016/j.carbpol.2021.117636

Gao, H.-X., He, Z., Sun, Q., He, Q., and Zeng, W.-C. (2019). "A functional polysaccharide film forming by pectin, chitosan, and tea polyphenols," *Carbohydrate Polymers* 215, 1-7. DOI: 10.1016/j.carbpol.2019.03.029

Gomaa, E. Z. (2017). "Silver nanoparticles as an antimicrobial agent: A case study on *Staphylococcus aureus* and *Escherichia coli* as models for Gram-positive and Gram-negative bacteria," *The Journal of General and Applied Microbiology* 63(1), 36-43. DOI: 10.2323/jgam.2016.07.004

Gong, X., Jadhav, N. D., Lonikar, V. V., Kulkarni, A. N., Zhang, H., Sankapal, B. R., Ren, J., Xu, B. B., Pathan, H. M., Ma, Y., Lin, Z., Witherspoon, E., Wang, Z., and Guo, Z. (2024). "An overview of green synthesized silver nanoparticles towards bioactive antibacterial, antimicrobial and antifungal applications," *Advances in Colloid and Interface Science* 323, article 103053. DOI: 10.1016/j.cis.2023.103053

Han, Z., Gong, Q., Huang, S., Meng, X., Xu, Y., Li, L., Shi, Y., Lin, J., Chen, X., Li, C., Ma, H., Liu, J., Zhang, X., Chen, D., and Si, J. (2023). "Machine learning uncovers accumulation mechanism of flavonoid compounds in *Polygonatum cyrtonema* Hua," *Plant Physiology and Biochemistry* 201, article 107839. DOI: 10.1016/j.plaphy.2023.107839

Hussain, Z., Jahangeer, M., Rahman, S. u., Ihsan, T., Sarwar, A., Ullah, N., Aziz, T., Alharbi, M., Alshammari, A., and Alasmari, A. F. (2023). "Synthesis of silver nanoparticles by aqueous extract of *Zingiber officinale* and their antibacterial activities against selected species," *Polish Journal of Chemical Technology* 25(3), 23-30. DOI: 10.2478/pjct-2023-0021

Iezzi, L., Vilardi, G., Saviano, G., and Stoller, M. (2022). "On the equipment design of a spinning disk reactor for the production of novel nano silver in amorphous zeolite particles," *Chemical Engineering Journal* 449, article 137864. DOI: 10.1016/j.cej.2022.137864

Khin, M. N., Ahammed, S., Aziz, T., Al-Asmari, F., Sameeh, M. Y., Cui, H., and Lin, L. (2024). "Characterization of composite film containing polyvinyl alcohol cross-linked with dialdehyde cellulose using citric acid as a catalyst for sustainable packaging," *Packaging Technology and Science* 37(10), 975-987. DOI: 10.1002/pts.2841

Li, Y., Sang, Y., Yu, W., Zhang, F., and Wang, X. (2023). "Antibacterial actions of Ag nanoparticles synthesized from *Cimicifuga dahurica* (Turcz.) Maxim. and their application in constructing a hydrogel spray for healing skin wounds," *Food Chemistry* 418, article 135981. DOI: 10.1016/j.foodchem.2023.135981

Liang, D., Lin, F., Yang, G., Yue, X., Zhang, Q., Zhang, Z., and Chen, H. (2015). "Advantages of immersion freezing for quality preservation of litchi fruit during frozen storage," *LWT - Food Science and Technology* 60(2, Part 1), 948-956. DOI: 10.1016/j.lwt.2014.10.034

Liao, M., Pan, Y., Fu, X., Wu, S., Gan, S., Wu, Z., Zhao, H., Zheng, W., Cao, Y., Zhou, W., and Dong, X. (2023). "Electrospun polylactic acid nanofiber film modified by silver oxide deposited on hemp fibers for antibacterial fruit packaging," *International Journal of Biological Macromolecules* 253, article 126569. DOI: 10.1016/j.ijbiomac.2023.126569

Lyu, L., Bi, Y., Li, S., Xue, H., Zhang, Z., and Prusky, D. B. (2019). "Early defense responses involved in mitochondrial energy metabolism and reactive oxygen species accumulation in harvested muskmelons infected by *Trichothecium roseum*," *Journal of Agricultural and Food Chemistry* 67(15), 4337-4345. DOI: 10.1021/acs.jafc.8b06333

Mao, L., Wang, C., Yao, J., Lin, Y., Liao, X., and Lu, J. (2023). "Design and fabrication of anthocyanin functionalized layered clay/poly(vinyl alcohol) coatings on poly(lactic acid) film for active food packaging," *Food Packaging and Shelf Life* 35, article 101007. DOI: 10.1016/j.fpsl.2022.101007

Mohaghegh, S., Osouli-Bostanabad, K., Nazemiyeh, H., Javadzadeh, Y., Parvizpur, A., Barzegar-Jalali, M., and Adibkia, K. (2020). "A comparative study of eco-friendly silver nanoparticles synthesis using *Prunus domestica* plum extract and sodium citrate as reducing agents," *Advanced Powder Technology* 31(3), 1169-1180. DOI: 10.1016/j.apt.2019.12.039

Montagut, D. C., Bueno, Y., Vesga, L. C., Stashenko, E. E., and Mendez-Sanchez, S. C. (2022). "*Cymbopogon flexuosus* (nees ex steud.) w. watson essential oil effect on mitochondrial bioenergetics," *Journal of Essential Oil Research* 34(3), 233-239. DOI: 10.1080/10412905.2022.2050315

Na-Phatthalung, W., Keaonaborn, D., Jaichuedee, J., Keawchouy, S., Sinyoung, S., and Musikavong, C. (2022). "Effect of silver nanoparticles and chlorine reaction time on the regulated and emerging disinfection by-products formation," *Environmental Pollution* 292, article 118400. DOI: 10.1016/j.envpol.2021.118400

Nie, X., Wang, L., Wang, S., Yu, N., Lu, Y., Lyu, W., and Meng, X. (2023). "*In vitro* hypoglycemic and antioxidant activities of steamed *Polygonatum cyrtonema* Hua with various steaming degrees: Relationship with homoisoflavonoids," *Food Bioscience* 53, article 102518. DOI: 10.1016/j.fbio.2023.102518

Pan, J., Ni, Z.-J., Thakur, K., Khan, M. R., Zhang, J.-G., and Wei, Z.-J. (2025). "Incorporation of *Polygonatum cyrtonema* extracts of NADES into chitosan/soybean isolate protein films: Impact on sweet cherry storage quality," *Food Chemistry* 463, article 141048. DOI: 10.1016/j.foodchem.2024.141048

Pinu, F. R. (2016). "Early detection of food pathogens and food spoilage microorganisms: Application of metabolomics," *Trends in Food Science & Technology* 54, 213-215. DOI: 10.1016/j.tifs.2016.05.018

Qi, F., Gao, X., Wang, C., Shuai, Y., Yang, L., Liao, R., Xin, J., Peng, S., and Shuai, C. (2022a). "*In situ* grown silver nanoparticles on tetrapod-like zinc oxide whisker for photocatalytic antibacterial in scaffolds," *Materials Today Sustainability* 19, article 100210. DOI: 10.1016/j.mtsust.2022.100210

Qi, Z., Xie, P., Yang, C., Xue, X., Chen, H., Zhou, H., Yuan, H., Yang, G., and Wang, C. (2023). "Developing fisetin-AgNPs incorporated in reinforced chitosan/pullulan composite-film and its application of postharvest storage in litchi fruit," *Food Chemistry* 407, article 135122. DOI: 10.1016/j.foodchem.2022.135122

Qi, Z., Xue, X., Xu, X., Zhou, H., Li, W., Yang, G., and Xie, P. (2022b). "Detoxified and antimicrobial-enhanced olive mill wastewater phenols capping ZnO nanoparticles incorporated with carboxymethyl cellulose for fresh strawberry preservation," *Postharvest Biology and Technology* 188, article 111891. DOI: 10.1016/j.postharvbio.2022.111891

Qi, Z., Xue, X., Zhou, H., Yuan, H., Li, W., Yang, G., Xie, P., and Wang, C. (2022c). "The aqueous assembly preparation of OPs-AgNPs with phenols from olive mill wastewater and its mechanism on antimicrobial function study," *Food Chemistry* 376, article 131924. DOI: 10.1016/j.foodchem.2021.131924

Saratale, G. D., Saratale, R. G., Cho, S.-K., Ghodake, G., Bharagava, R. N., Park, Y., Mulla, S. I., Kim, D.-S., Kadam, A., Nair, S., and Shin, H.-S. (2020). "Investigation of photocatalytic degradation of reactive textile dyes by *Portulaca oleracea*-functionalized silver nanocomposites and exploration of their antibacterial and antidiabetic potentials," *Journal of Alloys and Compounds* 833, article 155083. DOI: 10.1016/j.jallcom.2020.155083

Sathiyaseelan, A., Saravanakumar, K., Mariadoss, A. V. A., and Wang, M.-H. (2020). "Biocompatible fungal chitosan encapsulated phytogenic silver nanoparticles enhanced antidiabetic, antioxidant and antibacterial activity," *International Journal of Biological Macromolecules* 153, 63-71. DOI: 10.1016/j.ijbiomac.2020.02.291

Shi, C., Zhou, A., Fang, D., Lu, T., Wang, J., Song, Y., Lyu, L., Wu, W., Huang, C., and Li, W. (2022). "Oregano essential oil/β-cyclodextrin inclusion compound polylactic acid/polycaprolactone electrospun nanofibers for active food packaging," *Chemical Engineering Journal* 445, article 136746. DOI: 10.1016/j.cej.2022.136746

Silva, G. M. C., Morales, L. M. M., Santana, D. B., Santa-Catarina, C., and Oliveira, J. G. d. (2024). "The alternative respiration is linked with the ascorbate synthesis capacity in climacteric and non-climacteric fruit mitochondria," *Postharvest Biology and Technology* 210, article 112780. DOI: 10.1016/j.postharvbio.2024.112780

Sun, Y., Sun-Waterhouse, D., Cui, C., Feng, Y., and Wang, W. (2020). "Utilization of undesirable heat-induced precipitates/sediments in soy sauce production to fabricate

nanoparticles for curcumin delivery," *LWT* 130, article 109551. DOI: 10.1016/j.lwt.2020.109551

Ullah, S., Shah, S. W. A., Qureshi, M. T., Hussain, Z., Ullah, I., Kalsoom, U.-e., Rahim, F., Rahman, S. S. u., Sultana, N., and Khan, M. K. (2021). "Antidiabetic and hypolipidemic potential of green AgNPs against diabetic mice," *ACS Applied Bio Materials* 4(4), 3433-3442. DOI: 10.1021/acsabm.1c00005

Wu, Z., Tang, S., Deng, W., Luo, J., and Wang, X. (2021). "Antibacterial chitosan composite films with food-inspired carbon spheres immobilized AgNPs," *Food Chemistry* 363, article 130342. DOI: 10.1016/j.foodchem.2021.130342

Wu, Z., Zhang, Z., Song, X., Peng, W., Zhao, X., Zhao, H., Liang, D., Huang, C., and Duan, Q. (2024). "A silver nanoparticles-polylactic acid microspheres/polylactic acid-thermoplastic polyurethane nanofibers hierarchical antibacterial film," *Industrial Crops and Products* 207, article 117773. DOI: 10.1016/j.indcrop.2023.117773

Xu, D., Niu, Q., Gao, L., Wang, Q., Lan, C., Jiang, Z., and Qiao, F. (2025a). "Biocontrol potential of *Burkholderia gladioli* STPT16 on postharvest decay of litchi fruit caused by *Peronophythora litchii* and *Colletotrichum fructicola*," *Food Control* 168, article 110956. DOI: 10.1016/j.foodcont.2024.110956

Xu, M., Fang, D., Shi, C., Xia, S., Wang, J., Deng, B., Kimatu, B. M., Guo, Y., Lyu, L., Wu, Y., Cao, F., and Li, W. (2025b). "Anthocyanin-loaded polylactic acid/ quaternized chitosan electrospun nanofiber as an intelligent and active packaging film in blueberry preservation," *Food Hydrocolloids* 158, article 110586. DOI: 10.1016/j.foodhyd.2024.110586

Xue, H., Shen, L., Wang, X., Liu, C., Liu, C., Liu, H., and Zheng, X. (2019). "Isolation and purification of anthocyanin from blueberry using macroporous resin combined Sephadex LH-20 techniques," *Food Science and Technology Research* 25(1), 29-38. DOI: 10.3136/fstr.25.29

Yadav, S., Mehrotra, G. K., Bhartiya, P., Singh, A., and Dutta, P. K. (2020). "Preparation, physicochemical and biological evaluation of quercetin based chitosan-gelatin film for food packaging," *Carbohydrate Polymers* 227, article 115348. DOI: 10.1016/j.carbpol.2019.115348

Yang, G., Qi, Z., Shan, S., Lu, K., Zhou, J., Yang, L., and Tan, X. (2023). "Aqueous assembly of AgNPs with camellia seed cake polyphenols and its application as a postharvest anti-*Penicillium digitatum* agent via increasing reactive oxygen species generation," *Postharvest Biology and Technology* 206, article 112516. DOI: 10.1016/j.postharvbio.2023.112516

Yang, L.-X., Wu, Y.-N., Wang, P.-W., Huang, K.-J., Su, W.-C., and Shieh, D.-B. (2020). "Silver-coated zero-valent iron nanoparticles enhance cancer therapy in mice through lysosome-dependent dual programed cell death pathways: Triggering simultaneous apoptosis and autophagy only in cancerous cells," *Journal of Materials Chemistry B* 8(18), 4122-4131.

Yu, Y., Zhou, J., Chen, Q., Xie, F., Zhang, D., He, Z., Cheng, S., and Cai, J. (2024). "Self-reinforced multifunctional starch nanocomposite film for litchi fruit postharvest preservation," *Chemical Engineering Journal* 486, article 150262. DOI: 10.1016/j.cej.2024.150262

Zhang, Q., Yang, Z., and Su, W. (2024). "Review of studies on polysaccharides, lignins and small molecular compounds from three *Polygonatum* Mill. (Asparagaceae) spp. in crude and processed states," *International Journal of Biological Macromolecules*, 260, and 129511. DOI: 10.1016/j.ijbiomac.2024.129511

Zhang, Z., Liu, F., He, C., Yu, Y., and Wang, M. (2017). "Optimization of ultrasonic-assisted aqueous two-phase extraction of phloridzin from *Malus micromalus* Makino with ethanol/ammonia sulfate system," *Journal of Food Science* 82(12), 2944-2953. DOI: 10.1111/1750-3841.13958

Zhao, Y., Yan, D., Liu, J., Yang, S., Li, D., and Peng, L. (2023). "Vacuolar ATPase subunit H regulates growth development and pathogenicity of *Penicillium digitatum*," *Postharvest Biology and Technology* 199, article 112295. DOI: 10.1016/j.postharvbio.2023.112295

Article submitted: January 27, 2025; Peer review completed: February 22, 2025; Revised version received and accepted: April 18, 2025; Published: May 6, 2025.
DOI: 10.15376/biores.20.3.5279-5300